

# Photodetection in hybrid single layer graphene/fully coherent Ge island nanostructures selectively grown on Si nano-tip patterns

*Gang Niu<sup>1\*</sup>, Giovanni Capellini<sup>1,2</sup>, Grzegorz Lupina<sup>1</sup>, Tore Niermann<sup>3</sup>, Marco Salvalaglio<sup>4</sup>, Anna Marzegalli<sup>4</sup>, Markus Andreas Schubert<sup>1</sup>, Peter Zaumseil<sup>1</sup>, Hans-Michael Krause<sup>1</sup>, Oliver Skibitzki<sup>1</sup>, Michael Lehmann<sup>3</sup>, Francesco Montalenti<sup>4</sup>, Ya-Hong Xie<sup>5</sup>, Thomas Schroeder<sup>1,6</sup>*

1 IHP, Im Technologiepark 25, 15236 Frankfurt (Oder), Germany

2 Dipartimento di Scienze, Università Roma Tre, Viale Marconi 446, 00146 Rome, Italy

3 Technische Universität Berlin, Institut für Optik und Atomare Physik, Straße des 17. Juni 135, 10623 Berlin, Germany

4 L-NESS and Dept. of Materials Science, Università degli Studi di Milano-Bicocca, via Cozzi 55, I-20125 Milan, Italy

5 University of California at Los Angeles, Department of Materials Science and Engineering, Los Angeles, CA 90095-1595, USA

6 BTU Cottbus-Senftenberg, Konrad-Zuse-Str.1, 03046 Cottbus, Germany

## **KEYWORDS**

Germanium; selective epitaxy; elastic relaxation; graphene; photodetection

## ABSTRACT

Dislocation networks are one of the most principle sources deteriorating the performances of devices based on lattice-mismatched heteroepitaxial systems. We demonstrate here a technique enabling fully coherent Ge islands selectively grown on nano-tip patterned Si (001) substrates. The Si-tip patterned substrate, fabricated by complementary metal-oxide-semiconductor (CMOS) compatible nanotechnology, features ~50 nm wide Si areas emerging from a SiO<sub>2</sub> matrix and arranged in an ordered lattice. Molecular beam epitaxy (MBE) growths result in Ge nano-islands with high selectivity and having homogeneous shape and size. The ~850°C growth temperature required for ensuring selective growth has been shown to lead to the formation of Ge islands of high crystalline quality without extensive Si intermixing (with 91 at.% Ge). Nano-tip patterned wafers result in geometric, kinetic diffusion barrier intermixing hindrance confining the major intermixing to the pedestal region of Ge islands where kinetic diffusion barriers are however high. Theoretical calculations suggest that the thin SiGe layer at the interface plays nevertheless a significant role in realizing our fully coherent Ge nano-islands free from extended defects especially dislocations. Single layer graphene (SLG)/Ge/Si-tip Schottky junctions were fabricated and thanks to the absence of extended defect in Ge islands, they demonstrate high performance photodetection characteristics with responsivity and  $I_{on}/I_{off}$  ratio of ~45 mA/W and ~10<sup>3</sup>, respectively.

## 1. INTRODUCTION

Germanium (Ge), the semiconductor material at the base of the first transistor, is experiencing a renaissance due to its superior optoelectronic properties over that of silicon. The Ge/Si system has indeed been proposed for many different applications such as high-mobility complementary metal-oxide-semiconductor (CMOS) transistors<sup>1</sup>, memories<sup>2</sup>, thermoelectrics<sup>3</sup>, solar cells<sup>4</sup>, and monolithic integration of photonics with CMOS technology<sup>5</sup>. This renewed technological interest has fostered a wealth of studies on the heteroepitaxy of high quality Ge on Si in forms of both planar thin films and self-assembled nanometer-sized islands<sup>6</sup>. As a matter of fact, the growth of defect-free pure Ge/Si heterostructures is far from trivial. The relatively large lattice mismatch (4.2%) and thermal expansion coefficient (TEC) mismatch (130%) often lead to the introduction of dislocations and cracks. In addition, there is the strain-driven and surface energy-driven Ge-Si interdiffusion<sup>7</sup> causing difficulty in the control of the resulting heterostructure.

Among the methods proposed to tackle this problem<sup>6</sup>, approaches based on lithographic patterning of the Si substrates are recently under the spotlight. For the growth of thick Ge layer, micro-meter sized patterning has been proposed to limit threading dislocation propagation and crack formation<sup>8</sup>. For the growth of nanometers sized Ge islands, the selective epitaxy using nanostructured Si with “seeds” (possibly surrounded by almost “inert” material, e.g. SiO<sub>2</sub>), has been demonstrated to prevent plastic relaxation in Ge nano-islands. This selective epitaxy is in fact the basic idea of the approach commonly known as nanoheteroepitaxy (NHE)<sup>9-11</sup>. In NHE, thanks to the significant lateral deformation by strain partitioning between substrate and heteroepitaxial film nanostructure, the critical thickness for plastic relaxation of heteroepitaxial

systems can be largely increased, leading eventually to dislocation-free epitaxial layers when the lateral dimension of the “seed” pads is sufficient small (a few tens of nm).

Compared to traditional planar substrate approaches, using NHE one can obtain nanometric islands that are: i) elastically relaxed; ii) not connected by a continuous layer, and thus cracking or wafer bowing due to TEC mismatch is avoided; iii) with limited intermixing due to the small amount of silicon available on the surface; iv) with homogeneous size distribution; v) located in pre-determined position given by the lithographic pattern thus being easily integrable in a fabrication process and vi) strain engineered heterointerfaces with band-offsets at heterointerfaces different from the bulk case. The latter four features are of particular importance if NHE is benchmarked against other deposition techniques used to achieve Ge nano-islands such as the Stranski-Krastanov growth of Ge on planar Si substrates, which leads to randomly distributed, highly intermixed, size inhomogeneous self-assembled islands<sup>12-13</sup>. Pit-patterned Si substrates have been utilized to improve ordering and size uniformity<sup>14-18</sup> but with this approach Si-Ge intermixing is not prevented owing to the rather high process temperature required to achieve selectivity and high crystal quality<sup>15,17</sup>.

In prior studies, we have shown chemical vapor deposition (CVD) selective growth of Ge islands on Si nano-pillars<sup>19-21</sup> or compliant nano-mesas<sup>22-23</sup>. More recently, defect free Ge nano-islands have been achieved on free-standing Si nano-mesas<sup>24</sup>. The achievement of coherent Ge/Si interface without misfit dislocation network is especially important for device applications with charge carrier transport across the interface (e.g. tunnel field effect transistors, TFET) and opens new ways for band offset engineering. However, for Ge/Si-mesa approach, a SiGe buffer layer is needed to be additionally interposed between Ge and Si to realize the coherent growth<sup>24-25</sup>.

In this study, we demonstrate molecular beam epitaxy (MBE) selective growth of fully coherent Ge islands on nano-tip patterned Si (001) substrates. We show that the high temperature needed to achieve perfect selectivity and good crystalline quality, does not lead to extensive Ge-Si intermixing. Only limited intermixing is observed, which is confined to the island pedestal region leaving the rest of the island being nearly pure Ge. Moreover, thanks to the strain partitioning between Ge and Si tips, the thin intermixing layer has a beneficial role to prevent the formation of misfit dislocations (MDs) at the advantage of a fully elastic relaxation. We shall see the key enabler of this peculiar growth mode is the shape and size of the patterned Si substrate used as “seed” for the selective epitaxy. The beneficial influence of this innovative approach on optoelectronic materials properties is finally demonstrated by photodetection in hybrid single layer graphene (SLG) / Ge island / Si-tip nanostructures.

## 2. EXPERIMENTAL SECTION

Before the introduction of the Si-tip substrate into the MBE chamber, it was chemically cleaned by the following procedure: 1) 10s immersing in Piranha solution of H<sub>2</sub>SO<sub>4</sub> (98 wt%):H<sub>2</sub>O<sub>2</sub> (30wt%)=5:3) and 10s rinsing in de-ionized (DI) H<sub>2</sub>O; 2) 10s dipping in diluted HF (0.5 wt%) and 3) drying with N<sub>2</sub> gas. We note here that the dipping duration in HF was optimized to avoid over-etching of the SiO<sub>2</sub> around Si nano-tip. A pre-baking at a substrate temperature of 850°C was performed for 5 min in a DCA MBE chamber with a base pressure of 5×10<sup>-10</sup> mbar to remove the native oxide on the Si seeds. After the growth, the Ge morphology was examined by atomic force microscopy (AFM) in tapping mode (Veeco CP-II, high resolution Si tip with radius of curvature of 2 nm) and scanning electron microscopy (SEM, Zeiss Nvision 40). Out-of-plane and in-plane X-ray diffraction (XRD) measurements were performed using a Rigaku Smartlab diffractometer with a 9 kW rotating anode (Cu Kα1,

$\lambda=1.5406 \text{ \AA}$ ). Micro-Raman spectroscopy was carried out by employing a Renishaw Raman system with a 514 nm laser. The diameter of the laser spot is  $\sim 0.9 \text{ \mu m}$ . The sample was also prepared by mechanical polishing and Ar ion milling for transmission electron microscopy (TEM). The TEM measurements were performed using the FEI TITAN 80-300 Berlin Holography Special operated at 300 kV. The energy-dispersive X-ray spectroscopy (EDX) measurements were performed using a FEI Osiris operated at 200 kV. Numerical calculations were performed by solving the elastic problem by finite-element method (FEM) to gain insight of the strain relaxation mechanism of Ge islands on Si tips. SLG/Ge/Si-tip nanostructure was fabricated by transferring commercially available CVD graphene patches ( $1 \times 1 \text{ cm}^2$ ) onto the Ge/Si-tip substrate. The transfer was accomplished using PMMA support layers and wet Cu etching<sup>26</sup>. An Au metal was subsequently deposited on SLG/SiO<sub>2</sub> using electron beam DC sputtering to serve as the top contact and Ag paste was used as the bottom contact. The I-V characterizations were performed using a Keithley 4200 semiconductor analyzer. Both a 532 nm laser and a 1064 nm laser with a diameter of  $\sim 1.1 \text{ \mu m}$  were employed as the illumination light.

### 3. RESULTS AND DISCUSSION

The fabrication process of the nano-tip patterned Si wafer<sup>27</sup> is shown in Figure 1 (periphery part). At first the Si tips were realized by advanced lithography and reactive ion etching technologies available in standard Si CMOS processing lines (see Figure S1a in Supplementary Information). The tips are arranged in a two-dimensional square array with tip-tip spacing being  $\sim 1.41 \text{ \mu m}$  (areal density  $5 \times 10^7 \text{ cm}^{-2}$ ). A SiO<sub>2</sub> layer was subsequently grown by plasma enhanced chemical vapor deposition (PECVD) to fill the spaces between the tips and eventually completely cover the Si tips. Chemical-mechanical polishing (CMP) was carried out to expose the crystalline Si seeds of approximately 50 nm diameter (see Figure S1b in Supplementary

Information). It is noted that the duration of the CMP step can be used to control the surface area of the crystalline Si seed openings (with a minimum of  $\sim 5$  nm in diameter) and thus the nucleation size for subsequent Ge heteroepitaxy. Figure 1 (center part) shows a cross-sectional transmission electron microscopy (TEM) image of a single Si tip surrounded by SiO<sub>2</sub>.

Ge was grown using electron-beam evaporation for 45 minutes at 850°C and at a growth rate of  $\sim 0.02$  nm/s. Figure 2a displays a  $25 \mu\text{m} \times 25 \mu\text{m}$  atomic force microscopy (AFM) image exhibiting the highly ordered selective growth of Ge nano-islands on top of the Si nano-tips. In this image we can see that all the Si tips have seeded the nucleation of Ge islands while only one cluster has formed outside (see arrow). A statistical analysis on different images of the same size has shown a density of islands nucleated on top of the SiO<sub>2</sub> surface equal to  $\sim 2 \times 10^5 \text{ cm}^{-2}$ . This value is in good agreement with the prediction of nucleation theory for the stable Ge cluster density (i.e. cluster density maximum before coalescence) over SiO<sub>2</sub> surface at 850°C, which is  $\sim 9 \times 10^5 \text{ cm}^{-2}$  (Supporting Information). As pointed out by Han *et al.*<sup>28</sup> for the Ge growth on SiO<sub>2</sub> masked Si substrates, the selectivity occurs when the adatom lifetime on the SiO<sub>2</sub> surface is short enough so that they cannot form a critical nucleus before being desorbed. For increasing substrate temperature, the Ge adatoms over SiO<sub>2</sub> surface experience shortening residence time thus being in desorption (as opposed to incorporation) dominated growth mode<sup>29</sup>. At the growth temperature of 850°C, Ge adatom diffusion length over SiO<sub>2</sub> surface (i.e. average migration distance before desorption) can be estimated to only  $L \sim 0.44$  nm (Supporting Information). Figure 2b illustrates the selective growth mechanism for Ge/Si-tip system. Considering that the desorption energy of Ge from Si (001) (4.25 eV) is much higher than that from SiO<sub>2</sub> (0.44 eV)<sup>28, 30</sup>, at high growth temperature of 850°C, the Ge adatoms “stick” only on exposed Si seeds area while the Ge adatoms arriving on SiO<sub>2</sub> area desorb very quickly from the SiO<sub>2</sub> surface before

they can form stable clusters, due to their very short diffusion length of only 0.44 nm. As a consequence, the growth selectivity presented here can be realized on any pattern, with arbitrary distance and density of the nucleation seeds if a sufficiently high deposition temperature is used. On the contrary other methods are highly “pattern sensitive”. As an example, in the selective growth mechanism reported in Ge/pit-patterned Si system, the pit can trap all the deposited Ge only when the Ge adatom migration length is much longer than the pit periodicity<sup>31</sup>, or in CVD-based methods the loading effect plays a major role<sup>32</sup>.

Figure 2c shows a three dimensional (3D) rendering of a  $10\ \mu\text{m} \times 10\ \mu\text{m}$  AFM image of the same sample. The image shows high shape and size homogeneity of islands having an average height of  $58.6 \pm 2.5\ \text{nm}$ . The mean height of Ge nano-islands is approximately consistent with the thickness estimated by growth time multiplied by growth rate (calibrated using Ge growth on a planar Si substrate). The diameter of Ge nano-islands ( $\sim 120\ \text{nm}$ ) is larger than that of the Si-tip opening ( $\sim 50\ \text{nm}$ ), indicating that Ge nano-islands undergo both vertical and lateral growth (see Figure S2 in Supplementary Information). The total volume of Ge in nano-islands per unit area ( $\mu\text{m}^2$ ) is  $\sim 2.3 \times 10^5\ \text{nm}^3$  which is significantly less ( $>200$  times) than the volume per  $\mu\text{m}^2$  of evaporated Ge,  $\sim 5.4 \times 10^7\ \text{nm}^3$ . These results confirm the above-described desorption-dominated growth mode of Ge over  $\text{SiO}_2$  surface. Figure 2d exhibits an AFM surface-angle image on four Ge nano-islands allowing to visualize the sidewall angle of Ge nanostructures<sup>33-34</sup>. It can be observed in Figure 2d that Ge nano-islands display a homogenous “rocket head” shape with a small flat plateau on top (blue) and side wall (red) inclination angle is  $\sim 50^\circ$ . No well-defined faceting is observed.

The AFM results were complemented by a TEM study in order to further investigate the morphology, structure, and composition of Ge/Si-tip. Figure 3a displays a cross-sectional high



resolution TEM (HRTEM) image of a single Ge island grown on the Si-tip (for a TEM image with larger scale see Figure S3 in Supporting Information). It can be seen that the Ge cluster features a hemispherical shape without any distinguishable facet, thus confirming the AFM results (Figure 2c), contrary to the observed pyramidal, faceted-dome, or barn shapes<sup>17, 35-37</sup> in Ge islands grown on planar or pits-patterned Si at lower temperatures (400°C~600°C). Similar round shape was obtained for Ge islands grown<sup>23</sup> or annealed<sup>21</sup> at higher temperatures (800°C~900°C). The lack of facets at higher temperature is a direct result of entropy playing a more prominent role over that of facet energy. From TEM studies with a statistical analysis on different Ge islands, it can be concluded that the islands are free from extended defects such as threading dislocations, stacking faults (SFs), and micro-twins. In particular, careful HRTEM studies (Figure 3b) were carried out focusing on the center of Ge nano-islands (around point 3 in Figure 3a) where the misfit strain is the highest. The absence of dislocation segments from Figure 3b implies the structures are completely dislocation-free.

Insight in the composition of the islands are given by EDX measurements reported in Figure 3c, which shows a compositional map for Ge (blue) and Si (red) atoms. An EDX map of oxygen element was also obtained and shown in Figure S4 in Supporting Information. First we notice that the Si-tip is dome-like at the top region. We note that this deformation occurs during the pre-baking at >800°C (i.e. before the Ge growth, see Figure S5) due to desorption of volatile SiO formed following the reaction between Si-tip surface and the surrounding SiO<sub>2</sub>:  $\text{Si(s)} + \text{SiO}_2\text{(s)} \rightarrow 2\text{SiO(g)}$ <sup>38</sup>. Ge covers this Si-dome by filling the interspace between the Si-dome and surrounding SiO<sub>2</sub>. This filling is believed to be the origin of the SF observed at the shoulder of the Si tip (see arrow in Figure 3a): the SF is formed owing to a defect on the SiO<sub>2</sub> surface<sup>39-40</sup>. It can be also noticed that the blue color at the edge of the Ge island fades out indicating a decrease

of Ge concentration, which is related to the formation of a Ge oxide layer on the Ge islands surface. We also note here that a low pre-baking temperature ( $\sim 750^\circ\text{C}$ ) cannot completely remove the native  $\text{SiO}_2$  on Si tips and thus leading to additional defects like SFs (see Figure S6).

As stated before, epitaxial growth of Ge directly over Si is often associated with significant Si-Ge intermixing, leading to altered strain field especially in non-planar growths. To assess the extent of such intermixing, we perform an EDX line profile in the island at the nanometric scale. Figure 3d shows a line profile passing through the points 1-5 marked in Figure 3a. In the Ge island (point 1 and 2), the Ge atomic concentration is  $\sim 84\%$ , Si is  $\sim 8\%$ , and O is  $\sim 8\%$ . The oxygen contribution arises from the TEM lamella oxidation. The island is therefore formed by  $\sim 91\%$  Ge with only  $\sim 9\%$  Si. This is a quite surprising results considering the high growth temperature used. As a matter of fact, the Ge growth at similarly high temperatures ( $800\text{-}850^\circ\text{C}$ ) on pit-patterned<sup>16-17</sup>, pillar patterned<sup>21</sup>, or unpatterned substrates<sup>7</sup> results in Si-rich islands with Ge contents as low as 25%. On the contrary, a Ge-rich growth is here preserved thanks to the very limited extension of the surfacing Si regions and a nanowire-like shape of Si tips, which decrease the amount of Si atoms available for the intermixing. The interdiffusion process is limited to a narrow region across the Ge/Si interface, only  $2w$ -thick ( $w \sim 16$  nm, distance between point 2 and 3, Figure 3d), where the Ge concentration undergoes a gradual decrease from Ge island to Si-tip. Below point 3, the Ge concentration rapidly drops to 0% (point 4 and 5), suggesting no further Ge diffusion into Si-tip. This “geometric intermixing hindrance” effect shows a particular advantage of the Si-tip method for Ge growth on Si. Similar behavior has been reported for the thermal oxidation of nanometric scale  $\text{Si}^{41}$ . It is also noted here that the composition profiles (CPs) of Ge shown here (grown by MBE on nano-tip patterned Si wafers) with a Si-rich core in the bottom, is very different from the CPs seen in islands grown by MBE

on planar substrates, which are characterized by Si enriching the corners and Ge enriching the central regions and the top, forming a kind of a rosette structure<sup>42</sup>. In fact, the present CPs formed by MBE (on patterned Si), a non-equilibrium method, resembles the CPs formed by CVD growth (on planar Si), which is carried out in near-equilibrium conditions<sup>42</sup>. Furthermore, it is known that for the Ge growth on planar Si substrates, the introduction of dislocation can suppress the strain-induced SiGe intermixing<sup>43</sup>. In our dislocation-free Ge/Si-tip heterostructure realized by NHE, the SiGe intermixing is mainly due to thermodynamic reasons and limited by the “geometric intermixing hindrance” effect of Si tips (i.e. no Si diffusion into Ge islands by diffusion onto Ge island facets from neighboring Si substrate areas and only very limited Si diffusion through the Ge / Si pedestal area where activation barriers are high).

To gain insight into the strain distribution, selected area electron diffraction pattern analysis is performed. The pattern of the Ge/Si interface region, centered at point 3 with a diameter of approximately 75 nm, is shown in Figure 3e. It clearly demonstrates two different diffraction patterns corresponding to Si (outer) and Ge (inner), respectively. The inset shows an enlarged image of the Ge/Si (004) diffraction dots. The diffraction pattern confirms the single crystallinity and (001)-orientation of Ge islands on Si-tip. The extracted Si and Ge lattice constants are  $a_{\text{Ge}}=5.640\pm 0.020$  Å and  $a_{\text{Si}}=5.437\pm 0.020$  Å, respectively. Despite not being precise enough for more detailed strain analysis, these values indicate almost entirely strain-relaxed lattices of both Ge and Si. Furthermore, it can be observed that the Ge diffraction dot is much larger than that of Si and it diffuses towards Si diffraction dot, suggesting an interfacial SiGe layer with gradient Ge concentration.

More detailed crystallinity and strain analysis were carried out by XRD. In-plane XRD around Si (220) Bragg peak is shown in Figure 4a. The intense and sharp peak located at

$2\theta=47.30^\circ$  is the Si (220) Bragg diffraction. Interestingly, another peak ( $2\theta\sim 47.17^\circ$ , marked by an arrow) is present at the left foot of the Si (220) peak, corresponding to a Si component with in-plane tensile strain ( $a=5.446 \text{ \AA}$ ). Such in-plane tensile strain in Si nano-tips reveals the possible strain partitioning of misfit stress stored in Ge. We note here that it can also be related to the intrinsic strain in Si nano-tip induced by the residual stress in the surrounding PECVD-deposited  $\text{SiO}_2$  layer. Because in out-of-plane XRD, where no Ge-related signal was detected because of the limited amount of Ge, an additional peak appears at the high-angle shoulder of the Si (004) reflection (and such peak does not exist for the Si signal measured on un-patterned region), showing the corresponding out-of-plane compressive (thus in-plane tensile) strain of the tips (Figure S7). The diffraction peak located at  $2\theta=45.46^\circ$  is related to the Ge (220) reflection. Its position, quite close to that expected for relaxed Ge (dashed blue line in Figure 4a), indicates an in-plane lattice constant of the Ge islands of  $a=5.641 \text{ \AA}$ , i.e. a value slightly lower than that of Ge bulk ( $5.658 \text{ \AA}$ ), compatible with a fully relaxed  $\text{Ge}_{0.91}\text{Si}_{0.09}$  alloy, in excellent agreement with the TEM/EDX results. The slight asymmetry of the Ge (220) peak with shallower inclination on the high-angle side is due to the intermediate layer at Ge/Si interface with graded Ge concentration. An azimuthal  $\varphi$ -scan was carried out on the Ge (220) peak to analyze the mosaicity of Ge nano-islands and possible variations in lattice twist of the island ensemble. The observed full-width-of-half-maximum (FWHM) of  $0.27^\circ$  (see inset of Figure 4a) is mainly determined by the size of the Ge islands, thus indicating a good crystallinity and homogeneous epitaxial orientation of the Ge islands.

The AFM, TEM, and XRD results are also confirmed by Micro-Raman spectroscopy, here used to investigate the composition, the crystallinity and the strain of individual Ge nano-island. Figure 4b shows Raman spectra obtained on a Ge (001) substrate (black), on Ge islands (red),

and on the SiO<sub>2</sub> area between Ge islands (blue). The spectrum of Ge substrate as a reference shows a Raman line arising at ~300 cm<sup>-1</sup>, corresponding to the Ge-Ge Raman mode<sup>44</sup>. For the “on islands” spectrum, besides the strong Si line, two other lines appear at ~297 cm<sup>-1</sup> and at ~397 cm<sup>-1</sup>, corresponding to the Ge-Ge and Si-Ge modes, respectively<sup>44</sup>. For “between islands” spectrum, only a strong line at ~520 cm<sup>-1</sup> appears, corresponding to Si-Si mode of the Si substrate (SiO<sub>2</sub> mask is transparent). No Ge-Ge or Ge-Si related signal is observed in “between islands” spectrum, thus confirming the high selectivity of Ge on tip-patterned Si substrates. According to the Raman data we have determined the strain  $\varepsilon$  and composition  $x$  in Ge nano-islands<sup>44-45</sup>, which are ~0.1% and 0.85, respectively (Supporting Information and Figure S8). It has to be noted here that this estimation method is particularly suited for SiGe layers assuming that strain and composition are homogeneous in the layer while in our case a gradient of both factors exists particularly at the Ge/Si-tip interface, which is also reflected by the shape of Si-Ge peak with a large width of ~16 cm<sup>-1</sup>. Therefore, the values extracted above are average estimations in the entire Ge nano-island. These results are in good agreement with TEM, EDX and XRD analysis. The measured strain amount has to be considered due to both misfit and thermal stresses, the latter caused by the mismatch between the thermal expansion coefficient of the materials. Notice that, at the given deposition temperatures, such contribution is one order of magnitude lower than the lattice misfit strain. Figure 4c shows an intensity map of the Ge-Ge peak at 297 cm<sup>-1</sup> in a 6  $\mu\text{m} \times 6 \mu\text{m}$  area. This map confirms the high homogeneity of strain and composition of the island ensemble.

The experimental analysis gives evidence of the achievement of elastically relaxed, Ge nano-islands free from extended defects, such as MDs at the Ge/Si heterointerface, despite their high Ge content, featuring a relatively thin intermixed region.

To gain physical insight of the strain relaxation mechanism, we have performed numerical calculations, solving the elastic problem by FEM. The three-dimensional nanostructure geometry obtained from TEM image (Figure 3a) was mimicked in the FEM code assuming a rotational symmetry along the (001) axis. The resulting central cross section is shown in Figure 5a (the tip opening  $L$  is equal to 75 nm and the Ge island base is 120 nm). First, a uniform composition equal to  $x_{\text{Ge}}=90\%$  was considered in the Ge island ( $w=0$ ). The result is presented in the color map of Figure 5b where the in-plane strain-tensor component ( $\epsilon_{xx}$ ) values are plotted. It can be observed that the island free surfaces and the interfaces with  $\text{SiO}_2$  allow for a partial relaxation of the misfit strain. In particular, notice that tensile stressed region appears in Si ( $\epsilon_{xx} \sim 1\%$ ) while a symmetric region of compression ( $\epsilon_{xx} \sim -1\%$ ) is observed in Ge island. Such a strain partitioning is typical in Ge/Si finite area heterostructure<sup>24, 46</sup>. It is also worth noting here that, as shown in Figure 5b, the dome-like shape of the top of the Si-tip induces a particular strain distribution in the Ge island, with a compressive strain ( $\epsilon_{xx} \sim -1\%$ ) at the center region (blue) and a tensile strain ( $\epsilon_{xx} \sim 1\%$ ) at the Si-tip shoulder region (red) where Ge located between dome-like Si and the  $\text{SiO}_2$  wall. This is quite different from the case of Ge islands growth on a flat Si surface.

The compositional profile obtained from the EDX experiments (Figure 3d) was then included in the FEM calculations ( $w=16$  nm, see Supporting Information for other details). Figure 5a shows the Ge composition ( $x_{\text{Ge}}$ ) color map. The resulting deformation field, see the  $\epsilon_{xx}$  component plotted in Figure 5c, changes with respect to the uniform case (Figure 5b). The lowering of strain values around the tip and the overall enhancement in uniformity reveal the important contribution given by the intermixing process to the relaxation. These changes have consequences on the energetics of dislocation insertion.

We have investigated the tendency towards plastic relaxation by following the FEM-based procedure introduced in Ref. <sup>46</sup>, yielding the difference in energy ( $\Delta E$ ) between the system with or without dislocations. The dislocation-induced deformation was solved in 2D in the central section of the nanostructures, considering the effect of an infinitesimal  $60^\circ$ -dislocation segment placed at the interface (as in Ref. <sup>47</sup>). Then it was superimposed to the coherent elastic field in the same section that was obtained from a full 3D calculation (see Supporting Information for details).

In the  $w=0$  case (no intermixing), a dislocation segment was inserted at the central site of the Ge/Si interface. Calculations yield  $\Delta E=-30$  eV/nm. Insertion of a dislocation, thus, lowers the energy of the system. To treat the intermixed case, we placed the dislocation at the same site, corresponding to the  $x_{\text{Ge}}=0.45$  isoline (position 3 in Figure 3a). Notice that such dislocation positioning is energetically favored as it leads to significant relaxation both in the Ge-rich and in the Si-rich regions. The resulting in-plane strain tensor component is represented in Figure 5d. By integrating the elastic energy density we found  $\Delta E=-6$  eV/nm. Despite being extremely localized, the intermixing lowers by a factor of 5 the energetic gain provided by dislocation insertion. Furthermore, small changes in the nanostructure in terms of both geometry and composition can reverse the  $\Delta E$  sign. Actually, the  $L=75$  nm nanostructure is the largest one among the experimental samples. A broader analysis is reported in Figure 6, where we have indeed calculated  $\Delta E$  as a function of the tip opening-area and of the intermixed region width ( $L,w$ ). A black circle and a black square represent the two previously described calculations, with and without intermixing, respectively. The island base was scaled proportionally with  $L$ . The black line indicates the critical ( $L,w$ ) values for the onset of plasticity. The region described by ( $L,w$ ) values below the line (red area) corresponds to plastically relaxed structures, while for

(L,w) values above the critical line (blue region) the islands are predicted to be elastically relaxed. For the uniform case ( $w=0$ , strain field in Figure 5b), the critical opening area of the Si tip turns to be less than 30 nm. The delay in the dislocation onset due to the intermixing contribution (non-zero value of  $w$ ) is evident. The full L range experimentally realized and the statistical fluctuations of the composition profile, are highlighted within the green box. Notice that FEM calculations predict that this range (green box) covers the critical condition for the dislocation insertion (black line). By also considering that a calculation purely based on the energetics of initial and final configuration (as in our case), overestimates the tendency towards plastic relaxation (nucleation barriers are neglected), we conclude that the absence of dislocations found by TEM investigation is compatible with the model predictions and it can be explained as a consequence of the peculiar compositional profile. Notice that the thermal strain arising in the sample cooling at room temperature does not influence the plastic relaxation onset, as dislocations are nucleated at the growth temperature.

In order to verify the good quality of the Ge islands on Si-tip wafers and its impact on related optoelectronic devices, a hybrid SLG/Ge/Si-tip heterojunction was fabricated. Graphene has been employed as transparent electrode in many prototype optoelectronic devices such as photovoltaic modules, optical modulators, plasmonic devices as well as photodetectors<sup>48</sup>. Recently both graphene/Si<sup>49-50</sup> and graphene/Ge<sup>51</sup> Schottky junctions based photodetectors using planar Si and Ge substrates have been demonstrated. Here we fabricated a SLG/Ge/Si-tip device by transferring CVD graphene layer on fully coherent Ge islands grown on Si-tip substrates. More fabrication details are described in experimental section. Figure 7a shows a  $\mu$ -Raman spectrum of SLG/Ge/Si-tip heterostructure (see an illustration image in inset) using a 514 nm laser. It can be observed that besides the Si- ( $\sim 520\text{ cm}^{-1}$  and the second order  $\sim 960\text{ cm}^{-1}$ )<sup>52</sup>, Ge-



( $\sim 300 \text{ cm}^{-1}$ ) and SiGe-related ( $\sim 390 \text{ cm}^{-1}$ ) features (see Figure 4b for comparison), three additional peaks appear, belonging to graphene features, i.e. 2D-band at  $\sim 2677 \text{ cm}^{-1}$ , G-band at  $1585 \text{ cm}^{-1}$ , and the D-band at  $\sim 1344 \text{ cm}^{-1}$ . The intensity ratio between 2D and G peaks  $I_{2D}/I_G=2.6$ , proving the graphene is a single layer<sup>26</sup>.

Au and Ag contacts were subsequently fabricated (Figure 7a inset) for current-voltage (I-V) measurements at 300 K. The I-V curves show typical rectifying behavior (see Figure 7b), revealing the formation of a Schottky barrier between SLG and Ge/Si-tip. According to the thermionic emission theory, the rectifying behavior of an ideal Schottky barrier at forward bias can be described by<sup>50, 53</sup>  $J=J_s[\exp(eV/\eta k_B T)-1]$ , where  $J$  is the current density across the Schottky barrier,  $e$  is the electronic charge,  $V$  is the applied bias voltage,  $\eta$  is the ideality factor,  $k_B$  is the Boltzmann constant and  $T$  is the temperature in Kelvin.  $J_s$  is the saturation current density which can be expressed by  $J_s=A^*T^2\exp(-e\phi_{B0}/k_B T)$ , where  $A^*$  is the effective Richardson constant ( $\sim 66 \text{ A cm}^{-2}\text{K}^{-2}$  for Ge<sup>51</sup>) and  $\phi_{B0}$  is the zero bias barrier height of the SLG/Ge/Si-tip junction. By using the  $J_s$  value ( $4.2 \times 10^{-2} \text{ A cm}^{-2}$ ),  $\phi_{B0}$  of SLG/Ge/Si-tip was estimated to be 0.48 V, which is very close to the value obtained from SLG/bulk-Ge junction (0.46 V)<sup>51</sup> and that from SLG/Ge/planar-Si junction (0.42 V)<sup>54</sup>. The slight variation can be related to the possible deviation of the experimental Richardson constant from the theoretical one<sup>54-55</sup>.

Furthermore, compared to the curve in dark (black), I-V curve of the device under illumination with a 532 nm laser (red) shows an evident photocurrent response in reverse bias. The device displays a typical photovoltaic behavior showing an open-circuit voltage  $\sim 0.2 \text{ V}$  and short-circuit current  $\sim 0.2 \text{ mA}$ . The Figure 7b inset shows more details of photocurrent response ( $I_{\text{on}}-I_{\text{off}}$ ) at  $V=-0.2\text{V}$  to  $0.2\text{V}$  range with increasing laser power from  $P=4.8 \text{ mW}$  to  $P=72 \text{ mW}$ . In the SLG/Ge/Si-tip heterostructure, the Si-tip wafer is p-type with dopant concentration of  $\sim 10^{15}$

$\text{cm}^{-3}$  and Ge can be considered as intrinsic due to the absence of extended defects, which have an acceptor-like nature in Ge<sup>56-57</sup>. To illustrate the photovoltaic characteristics, Figure 7c shows a thermal equilibrium energy band diagram of the SLG/Ge/Si-tip photodetector under illumination at zero bias. Under the equilibrium condition, a built-in electric field is formed at the graphene/Ge interface vicinity. It is noted here that the transferred SLG layer is in general p-type doped therefore the Dirac cones of graphene shift slightly upward<sup>26</sup>. Under light, the electron-hole generation occurs and the electron-hole pairs are separated by the built-in electric field. The free electrons and holes move toward opposite directions therefore Fermi levels ( $E_F$ ) in graphene and in Ge/Si will be split by incident light<sup>51</sup>. The difference of the  $E_F$  levels is equal to the photovoltage which leads thus to photovoltaic current in the external circuit. Figure 7d shows the variation of short-circuit photocurrent (left, black curve) and responsivity (right, blue curve) as a function of the incident laser power. It can be observed that the photocurrent increases with increasing laser power. The  $I_{\text{on}}/I_{\text{off}}$  ratio is always in  $\sim 10^3$  range and reaches  $1.3 \times 10^3$  for  $P_{\text{laser}}=72$  mW. The responsivity is always in mA/W range and is  $\sim 45$  mA/W for  $P_{\text{laser}}=4.8$  mW. The measured characteristics are comparable with the photodetector based on SLG/Ge substrates<sup>51</sup>, indicating the high crystalline quality of the Ge islands. The responsivity of our SLG/Ge/Si-tip photodetector is much higher than several graphene based devices such as graphene/metal junctions (6.1 mA/W)<sup>48</sup>. Another key metric of photodetectors, the detectivity ( $D^*$ ) can be calculated by  $D^*=A^{1/2}R/(2eI_d)^{1/2}$ , where A is active area, R is responsivity, e is elementary charge ( $1.6 \times 10^{-19}$  C) and  $I_d$  is dark current. Considering the active area of  $\sim 2.0 \times 10^{-4}$   $\text{cm}^2$  (estimated junction area exposed to the light) and the  $I_d$  of  $3.8 \times 10^{-7}$  A,  $D^*$  of our SLG/Ge/Si-tip can be estimated to be  $1.82 \times 10^9$   $\text{cm Hz}^{1/2} \text{W}^{-1}$ , which is comparable with that of SLG/bulk-Ge<sup>51</sup> and bulk Si based photodetectors<sup>49</sup>.

In Figure 7d, the decrease of responsivity with increasing laser power could be attributed to light-induced Schottky barrier lowering, as already observed for Ge/Si photodetector (see e.g. Ref. <sup>58</sup> and references therein). Considering the 532 laser line is absorbed in a tiny region close to the SLG/Ge interface, photogenerated electrons could occupy the SLG/Ge interface states, thus modifying the band-bending and ultimately decreasing the electron-hole pair collection efficiency of the device. Remarkably, when the photodetector is illuminated using a laser emitting at a wavelength of 1064 nm, having a much larger penetration depth in Ge, the responsivity increases with the excitation power (see details in Figure S10 in Supporting Information). We point out that in this latter case the presence of any extended, acceptor-like defect in the Ge could generate a similar behavior (responsivity decreasing with increasing laser power), with electron filling of defect states at the Ge/Si heterointerface. Therefore the observed behavior, further corroborates the high epitaxial quality of the Ge nano-islands.

Furthermore, it is noted here that a reference sample composing of SLG/Si-tip without Ge islands was fabricated and characterized for comparison. It shows as well rectifying behavior of Schottky junctions but demonstrates almost no detectable photocurrent under the same illumination (see details in Figure S11 in Supporting Information). This confirms that the high performance photodetection characteristics of the SLG/Ge/Si-tip heterojunction correlate closely with the fully coherent Ge island nanostructures. Without threading (in islands) or misfit (at interface) dislocation networks (acceptor-like states) and with a low density of point defects in case of high temperature growth, Ge is well known to demonstrate outstanding optoelectronic properties in devices such as photodetectors.

#### **4. CONCLUSIONS**

In conclusion, we demonstrated in this study the selective growth of fully coherent Ge islands on nano-tip patterned Si (001) substrates by MBE. The well-ordered Ge nano-islands are highly homogeneous in both size and shape. An elevated growth temperature of 850°C is required for growth selectivity, and at such an elevated temperature Ge islands are still highly Ge-rich (~91 at.%). Theoretical calculations point out that, the shape and size of Si patterned substrate and the local SiGe intermixed layer occurring at the pedestal region of Ge island lead to completely elastic relaxation of Ge island hence fully coherent Ge is obtained. These results highlight the advantages of the Si-tip wafers for the growth of high quality Ge: i) perfect selectivity and absence of loading effect: any pattern, with arbitrary distance and density can be realized; ii) high deposition temperature and MBE results in crystalline quality: no H (compared to CVD method), reduced number of point defects affecting optical properties of Ge-rich islands; iii) “geometric intermixing hindrance” effect that confines intermixing to the pedestal region. Islands are Ge rich and the intermixing is beneficial for pure elastic relaxation; iv) the islands feature a MD-free interface with the substrate, a key aspect to nano-devices (e.g. TFET). Dislocation-free Ge islands lead to high performance photodetectors composed of hybrid SLG/Ge/Si-tip Schottky junctions, which show a responsivity and an  $I_{on}/I_{off}$  ratio of ~45 mA/W and  $\sim 10^3$ , respectively. From a more general point of view, this method can be probably transferred to the growth of high quality nano-islands of other functional materials (e.g. III-V and II-VI compounds) for various high performance devices and we can also bring the metal contacts in a reliable way (by aligning masks) to these nano-objects to serve as functional elements for macroscopic optoelectronic devices in future.

## FIGURES

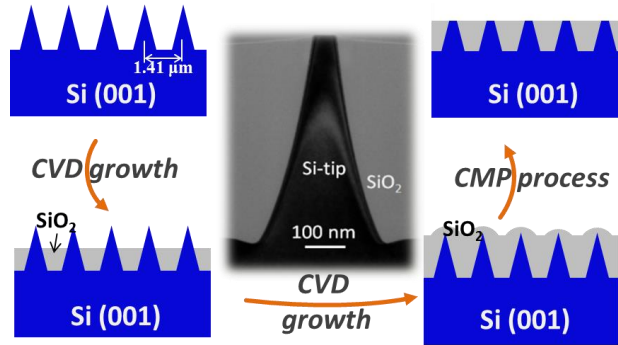


**Figure 1.** Counterclockwise: illustration of the fabrication process of tip-patterned Si substrate; center: a cross-sectional TEM image of the wafer showing a single Si tip. The Si-opening area at the top surface is  $\sim 50$  nm wide.

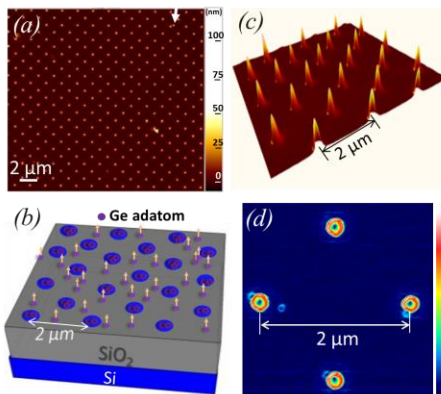


**Figure 2.** (a) a  $25 \mu\text{m} \times 25 \mu\text{m}$  AFM image of Ge islands on tip-patterned Si substrates: the arrow indicates an island nucleated on top of the  $\text{SiO}_2$  surface; (b) an illustration of selective growth mechanism of Ge on nano-tip patterned Si substrates; (c) a three-dimensional rendering of  $10 \mu\text{m} \times 10 \mu\text{m}$  AFM image; (d) a  $2.5 \mu\text{m} \times 2.5 \mu\text{m}$  AFM surface angle image showing the shape of Ge islands with the colors from blue to red indicating increasing sidewall angles. All AFM images are aligned along  $[110]$ -equivalent directions.

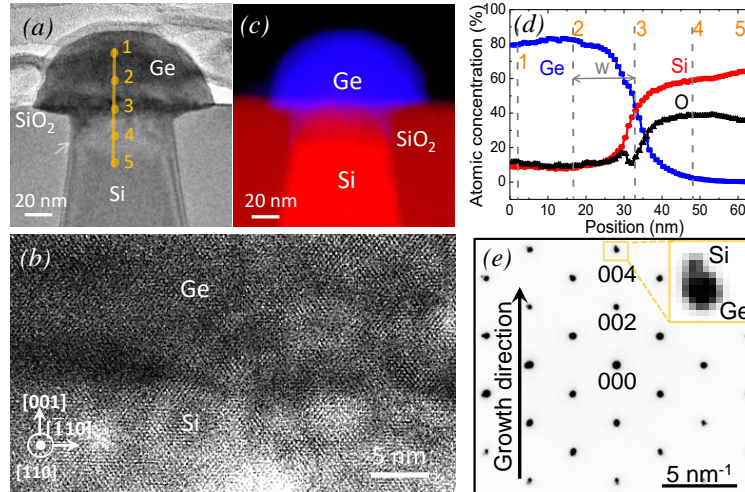


**Figure 3.** (a) A cross-sectional HRTEM image of a Ge nano-island on Si-tip substrate. The arrow marks a SF; (b) atomic resolution cross-sectional HRTEM image obtained around point 3 in panel (a) (central region of Ge/Si interface). (c) EDX map of Ge (blue) and Si (red) signals; (d) EDX line profile connecting points 1-5 in panel (a) showing the atomic concentration of Ge, Si and O; (e) an electron diffraction pattern around the Ge/Si interface and inset shows separated Si and Ge 004 diffraction dots.

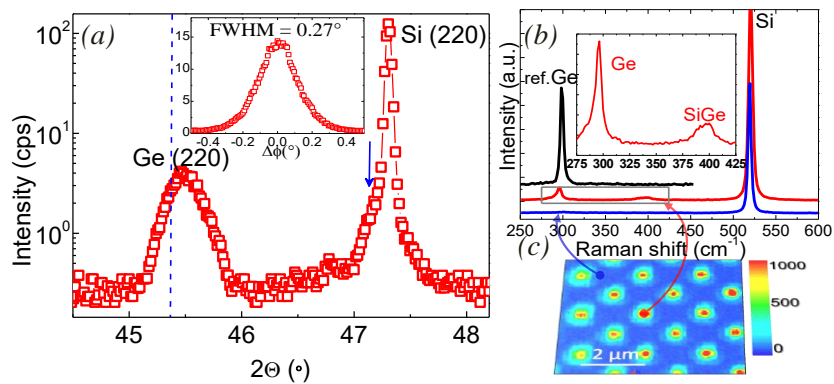


**Figure 4.** (a) In-plane XRD measurement around Si (220) Bragg peak. The dotted blue line shows the position of fully-relaxed Ge and the blue arrow indicates a peak related to residual tensile strain in the Si tips; inset image shows a  $\phi$  scan on Ge (220) reflection indicating a

FWHM=0.27°; (b)  $\mu$ -Raman spectra of a Ge substrate (black) and Ge/Si tips sample by on- (red) and between Ge islands (blue); the inset shows an enlarged picture of the squared region of the “on islands” spectrum; (c) a map of Ge peak intensity, the intensity increases from blue to red.

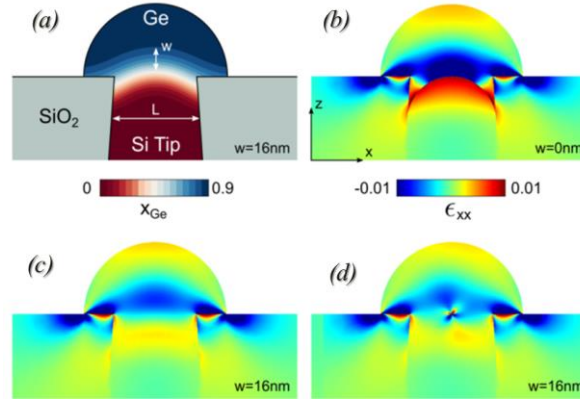


**Figure 5.** (a) Central section of the 3D structure geometry and color map of the compositional profile as included in the FEM calculations. (b) Color map of the  $\epsilon_{xx}$  strain component as obtained by FEM simulation in the case of uniform  $x_{Ge}=0.9$  composition. (c) Color map of the  $\epsilon_{xx}$  strain component as obtained by FEM simulation for the compositional profile described in (a). (d) same as in (c) with a dislocation segment inserted in the structure central section.

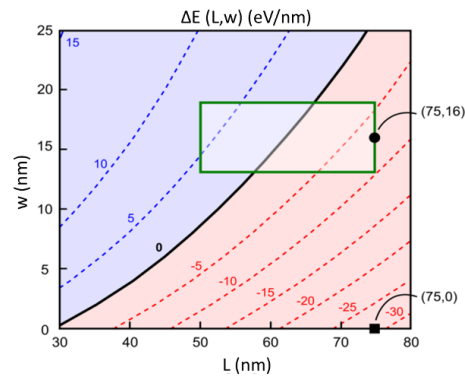


**Figure 6.** Phase diagram describing the onset of plasticity in the islands. Black line correspond to critical values of L and w ( $\Delta E = 0$ ), red region (below) correspond to overcritical islands (thus

undergoing both elastic and plastic relaxation) while for parameters in the blue region (above) island is predicted to be coherent (thus undergoing only elastic relaxation); The numbers on the dashed lines indicate the values of  $\Delta E$ , namely the difference in energy when a dislocation is present in the system, with respect to the coherent case. Green box included the experimental ranges of  $L$  and  $w$ . A black circle and a black square represent the calculations for (75,16) and (75,0), respectively.

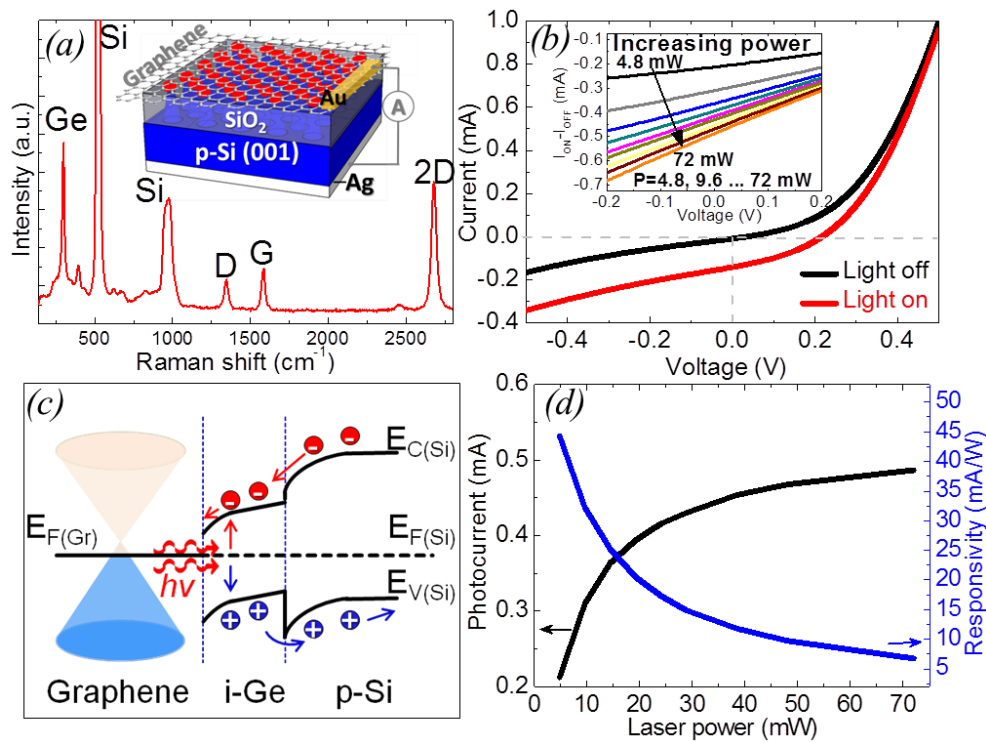


Figure 7 (a)  $\mu$ -Raman spectrum of SLG/Ge/Si-tip nanostructure using a  $\lambda=514\text{nm}$  laser on Ge islands region; Inset shows an illustration of sample structure details as well as the device structure for I-V measurements with top and bottom contacts of Au and Ag, respectively; (b) I-V characteristics of the SLG/Ge/Si-tip device shown in inset of (a) with black and red curves representing conditions under no light illumination and under light illumination with a  $\lambda=532\text{ nm}$  laser; Inset shows the photocurrent ( $I_{\text{on}}-I_{\text{off}}$ ) augmentation under illumination with increasing



laser power of 4.8 mW, 9.6 mW... and 72 mW; (c) Energy band diagram of the SLG/Ge/Si-tip photodetector under illumination at zero bias.  $E_F$  denotes the Fermi energy level;  $E_C$  and  $E_V$  are the conduction and valence bands, respectively. The graphene Dirac cones shift slightly upward because the transferred graphene sheet is normally p-type doped. (d) Dependence of short-circuit photocurrent and responsivity on the incident laser power.

## ASSOCIATED CONTENT

### Supporting Information.

Fabrication details of nano-tip patterned Si wafers, theoretical calculation of selective growth of Ge on SiO<sub>2</sub>-patterned Si, morphology of Ge islands by SEM images, Si-tip deformation after pre-baking process, specular XRD results of Ge islands, details of determination of strain and composition of SiGe alloy by Raman data, FEM calculation details and I-V measurements of SLG/Ge/Si-tip heterostructure using 1064 nm laser illumination and I-V characteristics of SLG/Si-tip Schottky junction will be shown. This material is available free of charge via the Internet at <http://pubs.acs.org>.

## AUTHOR INFORMATION

### Corresponding Author

\* Gang Niu, Email: [gang@ihp-microelectronics.com](mailto:gang@ihp-microelectronics.com)

### Author Contributions

G.N., G.C., Y.-H.X. and T.S. designed this work. G.N., G.C., G.L. T.S. and A. M. prepared the manuscript. G.N., G.C., G.L., T.N., M.A.S, P.Z., H.-M.K., O.S., M.L. and Y.-H.X. carried out

the experiments while M.S., A.M. and F.M. performed the theoretical calculation. All authors contributed in results analysis and discussion of the manuscript during the preparation. All authors have given approval to the final version of the manuscript.

### **Funding Sources**

This work is partly funded by the Deutsche Forschungsgemeinschaft (DFG) “DACH” project (project number: SCHR 1123/10-1).

### **Notes**

The authors declare no competing financial interest.

### **ACKNOWLEDGMENT**

The authors would like to thank Mirko Fraschke for the help of the tip-patterned wafers fabrication. We acknowledge Jens Katzer for the help on SEM measurements, Hans-Jürgen Thieme and Julia Kitzmann for technical assistance during the sample preparation and A. Cortinovis for preliminary FEM investigations.

### **REFERENCES**

- (1) Lee, M. L.; Fitzgerald, E. A.; Bulsara, M. T.; Currie, M. T.; Lochtefeld, A. Strained Si, SiGe, and Ge Channels for High-Mobility Metal-Oxide-Semiconductor Field-Effect Transistors. *J. Appl. Phys.* 2005, *97*, 011101.
- (2) Chang, T.-C.; Jian, F.-Y.; Chen, S.-C.; Tsai, Y.-T. Developments in Nanocrystal Memory. *Materials Today* 2011, *14*, 608-615.
- (3) Mingo, N.; Hauser, D.; Kobayashi, N. P.; Plissonnier, M.; Shakouri, A. “Nanoparticle-in-Alloy” Approach to Efficient Thermoelectrics: Silicides in SiGe. *Nano Lett.* 2009, *9*, 711-715.

- (4) Olson, J. M.; Friedman, D. J.; Kurtz, S., High-Efficiency III-V Multijunction Solar Cells. In *Handbook of Photovoltaic Science and Engineering.*, 2nd ed.; Luque, A.; Hegedus, S., Eds. John Wiley & Sons: **2010**; Chapter 9, pp 360-408.
- (5) Soref, R. The Past, Present, and Future of Silicon Photonics. *IEEE J. Sel. Topics Quantum Electron* 2006, *12*, 1678-1687.
- (6) Ye, H.; Yu, J. Germanium Epitaxy on Silicon. *Sci. Technol. Adv. Mater.* 2014, *15*, 024601.
- (7) Capellini, G.; De Seta, M.; Evangelisti, F. SiGe Intermixing in Ge/Si(100) Islands. *Appl. Phys. Lett.* 2001, *78*, 303-305.
- (8) Falub, C. V.; von Känel, H.; Isa, F.; Bergamaschini, R.; Marzegalli, A.; Chrastina, D.; Isella, G.; Müller, E.; Niedermann, P.; Miglio, L. Scaling Hetero-Epitaxy from Layers to Three-Dimensional Crystals. *Science* 2012, *335*, 1330-1334.
- (9) Zubia, D.; Hersee, S. D. Nanoheteroepitaxy: The Application of Nanostructuring and Substrate Compliance to the Heteroepitaxy of Mismatched Semiconductor Materials. *J. Appl. Phys.* 1999, *85*, 6492-6496.
- (10) Zubia, D.; Zaidi, S. H.; Hersee, S. D.; Brueck, S. R. J. Nanoheteroepitaxy: Nanofabrication Route to Improved Epitaxial Growth. *J. Vac. Sci. Tech. B* 2000, *18*, 3514-3520.
- (11) Luryi, S.; Suhir, E. New Approach to the High Quality Epitaxial Growth of Lattice - Mismatched Materials. *Appl. Phys. Lett.* 1986, *49*, 140-142.
- (12) Eaglesham, D. J.; Cerullo, M. Dislocation-Free Stranski-Krastanow Growth of Ge on Si(100). *Phys. Rev. Lett.* 1990, *64*, 1943-1946.
- (13) Kim, H. J.; Zhao, Z. M.; Liu, J.; Ozolins, V.; Chang, J. Y.; Xie, Y. H. A Technique for the Measurement of Surface Diffusion Coefficient and Activation Energy of Ge Adatom on Si(001). *J. Appl. Phys.* 2004, *95*, 6065-6071.

- (14) Zhong, Z.; Bauer, G. Site-Controlled and Size-Homogeneous Ge Islands on Prepatterned Si (001) Substrates. *Appl. Phys. Lett.* 2004, *84*, 1922-1924.
- (15) Zhang, J. J.; Hrauda, N.; Groiss, H.; Rastelli, A.; Stangl, J.; Schäffler, F.; Schmidt, O. G.; Bauer, G. Strain Engineering in Si via Closely Stacked, Site-Controlled SiGe Islands. *Appl. Phys. Lett.* 2010, *96*, 193101.
- (16) Zhang, J.; Rastelli, A.; Schmidt, O. G.; Bauer, G. Compositional Evolution of SiGe Islands on Patterned Si (001) Substrates. *Appl. Phys. Lett.* 2010, *97*, 203103.
- (17) Schüllli, T. U.; Vastola, G.; Richard, M. I.; Malachias, A.; Renaud, G.; Uhlík, F.; Montalenti, F.; Chen, G.; Miglio, L.; Schäffler, F.; Bauer, G. Enhanced Relaxation and Intermixing in Ge Islands Grown on Pit-Patterned Si(001) Substrates. *Phys. Rev. Lett.* 2009, *102*, 025502.
- (18) Capellini, G.; De Seta, M.; Spinella, C.; Evangelisti, F. Ordering Self-Assembled Islands without Substrate Patterning. *Appl. Phys. Lett.* 2003, *82*, 1772-1774.
- (19) Zaumseil, P.; Yamamoto, Y.; Bauer, A.; Schubert, M. A.; Schroeder, T. X-ray Characterization of Ge Epitaxially Grown on Nanostructured Si(001) Wafers. *J. Appl. Phys.* 2011, *109*, 023511.
- (20) Kozłowski, G.; Zaumseil, P.; Schubert, M. A.; Yamamoto, Y.; Bauer, J.; Matejova, J.; Schüllli, T.; Tillack, B.; Schroeder, T. Compliant Substrate versus Plastic Relaxation Effects in Ge Nanoheteroepitaxy on Free-Standing Si(001) Nanopillars. *Appl. Phys. Lett.* 2011, *99*, 141901.
- (21) Kozłowski, G.; Zaumseil, P.; Schubert, M. A.; Yamamoto, Y.; Bauer, J.; Schüllli, T. U.; Tillack, B.; Schroeder, T. Growth and Relaxation Processes in Ge Nanocrystals on Free-Standing Si(001) Nanopillars. *Nanotechnology* 2012, *23*, 115704.
- (22) Zaumseil, P.; Kozłowski, G.; Yamamoto, Y.; Bauer, J.; Schubert, M. A.; Schüllli, T. U.; Tillack, B.; Schroeder, T. Compliant Si Nanostructures on SOI for Ge Nanoheteroepitaxy—A

Case Study for Lattice Mismatched Semiconductor Integration on Si(001). *J. Appl. Phys.* 2012, *112*, 043506.

(23) Zaumseil, P.; Kozlowski, G.; Yamamoto, Y.; Schubert, M. A.; Schroeder, T. X-ray Characterization of Ge Dots Epitaxially Grown on Nanostructured Si Islands on Silicon-on-Insulator Substrates. *J. Appl. Cryst.* 2013, *46*, 868-873.

(24) Montalenti, F.; Salvalaglio, M.; Marzegalli, A.; Zaumseil, P.; Capellini, G.; Schüllli, T. U.; Schubert, M. A.; Yamamoto, Y.; Tillack, B.; Schroeder, T. Fully Coherent Growth of Ge on Free-Standing Si(001) Nanomesas. *Phys. Rev. B* 2014, *89*, 014101.

(25) Zaumseil, P.; Kozlowski, G.; Schubert, M. A.; Yamamoto, Y.; Bauer, J.; Schüllli, T. U.; Tillack, B.; Schroeder, T. The Role of SiGe Buffer in Growth and Relaxation of Ge on Free-Standing Si(001) Nano-Pillars. *Nanotechnology* 2012, *23*, 355706.

(26) Lupina, G.; Kitzmann, J.; Costina, I.; Lukosius, M.; Wenger, C.; Wolff, A.; Vaziri, S.; Östling, M.; Pasternak, I.; Krajewska, A.; Strupinski, W.; Kataria, S.; Gahoi, A.; Lemme, M. C.; Ruhl, G.; Zoth, G.; Luxenhofer, O.; Mehr, W. Residual Metallic Contamination of Transferred Chemical Vapor Deposited Graphene. *ACS Nano* 2015, *9*, 4776-4785.

(27) Mehr, W.; Wolff, A.; Frankenfeld, H.; Skaloud, T.; Höppner, W.; Bugiel, E.; Lärz, J.; Hunger, B. Ultra Sharp Crystalline Silicon Tip Array Used as Field Emitter. *Microelectron. Eng.* 1996, *30*, 395-398.

(28) Leonhardt, D.; Han, S. M. Energetics of Ge Nucleation on SiO<sub>2</sub> and Implications for Selective Epitaxial Growth. *Surf. Sci.* 2009, *603*, 2624-2629.

(29) Gomer, R. Diffusion of Adsorbates on Metal Surfaces. *Rep. Prog. Phys.* 1990, *53*, 917-1002.

- (30) Li, Q.; Krauss, J. L.; Hersee, S.; Han, S. M. Probing Interactions of Ge with Chemical and Thermal SiO<sub>2</sub> to Understand Selective Growth of Ge on Si during Molecular Beam Epitaxy. *J. Phys. Chem. C* 2007, *111*, 779-786.
- (31) Bollani, M.; Chrastina, D.; Fedorov, A.; Sordan, R.; Picco, A.; Bonera, E. Ge-rich Islands Grown on Patterned Si Substrates by Low-Energy Plasma-Enhanced Chemical Vapour Deposition. *Nanotechnology* 2010, *21*, 475302.
- (32) Yamamoto, Y.; Kozłowski, G.; Zaumseil, P.; Tillack, B. Low Threading Dislocation Ge on Si by Combining Deposition and Etching. *Thin Solid Films* 2012, *520*, 3216-3221.
- (33) Kamins, T. I.; Medeiros-Ribeiro, G.; Ohlberg, D. A. A.; Stanley Williams, R. Evolution of Ge Islands on Si(001) during Annealing. *J. Appl. Phys.* 1999, *85*, 1159-1171.
- (34) Grydlik, M.; Langer, G.; Fromherz, T.; Schäffler, F.; Brehm, M. Recipes for the Fabrication of Strictly Ordered Ge Islands on Pit-Patterned Si(001) Substrates. *Nanotechnology* 2013, *24*, 105601.
- (35) Medeiros-Ribeiro, G.; Bratkovski, A. M.; Kamins, T. I.; Ohlberg, D. A. A.; Williams, R. S. Shape Transition of Germanium Nanocrystals on a Silicon (001) Surface from Pyramids to Domes. *Science* 1998, *279*, 353-355.
- (36) Sutter, E.; Sutter, P.; Bernard, J. E. Extended Shape Evolution of Low Mismatch Si<sub>1-x</sub>Ge<sub>x</sub> Alloy Islands on Si(100). *Appl. Phys. Lett.* 2004, *84*, 2262-2264.
- (37) Marzegalli, A.; Zinovyev, V. A.; Montalenti, F.; Rastelli, A.; Stoffel, M.; Merdzhanova, T.; Schmidt, O. G.; Miglio, L. Critical Shape and Size for Dislocation Nucleation in Si<sub>1-x</sub>Ge<sub>x</sub> Islands on Si (001). *Phys. Rev. Lett.* 2007, *99*, 235505.
- (38) Gustaffsson, T.; Gusev, E. P.; Garfunkel, E.; Starodub, D. Silicon Oxide Decomposition and Desorption During the Thermal Oxidation of Silicon. *Surf. Rev. Lett.* 1999, *06*, 45-52.

- (39) Li, Q.; Pattada, B.; Brueck, S. R. J.; Hersee, S.; Han, S. M. Morphological Evolution and Strain Relaxation of Ge Islands Grown on Chemically Oxidized Si(100) by Molecular-Beam Epitaxy. *J. Appl. Phys.* 2005, *98*, 073504.
- (40) Tan, T. Y.; Gösele, U. Oxidation-Enhanced or Retarded Diffusion and the Growth or Shrinkage of Oxidation-Induced Stacking Faults in Silicon. *Appl. Phys. Lett.* 1982, *40*, 616.
- (41) Sun, K.; Zhang, W.; Li, B.; Lee, J. Y.; Xie, Y.-H.; Schroeder, T.; Katzer, J.; Wei, X.; Russell, T. P. Field Emission Tip Array Fabrication Utilizing Geometrical Hindrance in the Oxidation of Si. *IEEE Trans. Nanotechnol.* 2012, *11*, 999-1003.
- (42) Georgiou, C.; Leontiou, T.; Kelires, P. C. Shaping the Composition Profiles in Heteroepitaxial Quantum dots: Interplay of Thermodynamic and Kinetic effects. *AIP Adv.* 2014, *4*, 077135.
- (43) Leontiou, T.; Tersoff, J.; Kelires, P. C. Suppression of Intermixing in Strain-Relaxed Epitaxial Layers. *Phys. Rev. Lett.* 2010, *105*, 236104.
- (44) Capellini, G.; De Seta, M.; Busby, Y.; Pea, M.; Evangelisti, F.; Nicotra, G.; Spinella, C.; Nardone, M.; Ferrari, C. Strain Relaxation in High Ge Content SiGe Layers Deposited on Si. *J. Appl. Phys.* 2010, *107*, 063504.
- (45) Perova, T. S.; Wasyluk, J.; Lyutovich, K.; Kasper, E.; Oehme, M.; Rode, K.; Waldron, A. Composition and Strain in thin  $\text{Si}_{1-x}\text{Ge}_x$  Virtual Substrates Measured by micro-Raman Spectroscopy and X-Ray Diffraction. *J. Appl. Phys.* 2011, *109*, 033502.
- (46) Salvalaglio, M.; Montalenti, F. Fine Control of Plastic and Elastic Relaxation in Ge/Si Vertical Heterostructures. *J. Appl. Phys.* 2014, *116*, 104306.
- (47) Gatti, R.; Marzegalli, A.; Zinovyev, V. A.; Montalenti, F.; Miglio, L. Modeling the Plastic Relaxation Onset in Realistic SiGe Islands on Si (001). *Phys. Rev. B* 2008, *78*, 184104.

- (48) Koppens, F. H. L.; Mueller, T.; Avouris, P.; Ferrari, A. C.; Vitiello, M. S.; Polini, M. Photodetectors Based on Graphene, Other Two-Dimensional Materials and Hybrid Systems. *Nat Nanotechnol.* 2014, *9*, 780-793.
- (49) An, X.; Liu, F.; Jung, Y. J.; Kar, S. Tunable Graphene–Silicon Heterojunctions for Ultrasensitive Photodetection. *Nano Letters* 2013, *13*, 909-916.
- (50) Chen, C.-C.; Aykol, M.; Chang, C.-C.; Levi, A. F. J.; Cronin, S. B. Graphene-Silicon Schottky Diodes. *Nano Letters* 2011, *11*, 1863-1867.
- (51) Zeng, L.-H.; Wang, M.-Z.; Hu, H.; Nie, B.; Yu, Y.-Q.; Wu, C.-Y.; Wang, L.; Hu, J.-G.; Xie, C.; Liang, F.-X.; Luo, L.-B. Monolayer Graphene/Germanium Schottky Junction As High-Performance Self-Driven Infrared Light Photodetector. *ACS Appl. Mater. & Interfaces* 2013, *5*, 9362-9366.
- (52) Parker, J. H.; Feldman, D. W.; Ashkin, M. Raman Scattering by Silicon and Germanium. *Phys. Rev.* 1967, *155*, 712-714.
- (53) Xie, C.; Nie, B.; Zeng, L.; Liang, F.-X.; Wang, M.-Z.; Luo, L.; Feng, M.; Yu, Y.; Wu, C.-Y.; Wu, Y.; Yu, S.-H. Core–Shell Heterojunction of Silicon Nanowire Arrays and Carbon Quantum Dots for Photovoltaic Devices and Self-Driven Photodetectors. *ACS Nano* 2014, *8*, 4015-4022.
- (54) Khurelbaatar, Z.; Kil, Y.-H.; Shim, K.-H.; Cho, H.; Kim, M.-J.; Kim, Y.-T.; Choi, C.-J. Temperature Dependent Current Transport Mechanism in Graphene/Germanium Schottky Barrier Diode. *J. Semi. Technol. Sci.* 2015, *15*, 7-15.
- (55) Karataş, Ş.; Altı ndal, Ş.; Türüt, A.; Özmen, A. Temperature Dependence of Characteristic Parameters of the H-terminated Sn/p-Si(100) Schottky Contacts. *Appl. Surf. Sci.* 2003, *217*, 250-260.



- (56) Ismail, K. Effect of Dislocations in Strained Si/SiGe on Electron Mobility. *J. Vac. Sci. Technol. B* 1996, *14*, 2776-2779.
- (57) Shockley, W. Dislocations and Edge States in the Diamond Crystal Structure. *Phys. Rev.* 1953, *91*, 228.
- (58) Gity, F.; Daly, A.; Snyder, B.; Peters, F. H.; Hayes, J.; Colinge, C.; Morrison, A. P.; Corbett, B. Ge/Si Heterojunction Photodiodes Fabricated by Low Temperature Wafer Bonding. *Opt. Exp.* 2013, *21*, 17309-17314.

# Table of Contents Graphic

